Chapter 4

ANTARCTIC CIRCUMPOLAR CURRENT

1 Phenomenology

The Antarctic Circumpolar Current (ACC) is unique because of the combination of westerly wind stress at the surface and the absence of continental barriers along latitude lines (though there are proximate partial barriers). The response is a broad eastward geostrophic ACC flow, extending over ~ 1000 km meridionally (with embedded narrow ribbons of stronger flow) and $\sim 25,000$ km zonally, and reaching down to the bottom where the influence of topography is strong. There is also an equatorward Ekman flow (with transport to the left of the wind since $f < 0$), whose associated interior meridional overturning circulation (MOC) is called the Deacon Cell. Sverdrup balance is precluded for the ACC because there can be no balancing zonal pressure gradient for a geostrophic, zonally averaged meridional flow. Although the ACC is primarily wind-driven, it is enveloped in the global thermohaline circuit (Chap. 1, Figs. 5 and 7), and most likely there is important mutual coupling between the ACC and the diabatic aspects of the MOC in the Southern Ocean.

In Chaps. 1 and 2 we saw various depictions of the ACC region:

- Mariner's chart and an OGCM solution for surface currents (Chap. 1, Figs. 2 and 12)
- Surface winds (Chap. 2, Figs. 2-3)
- Ekman and Stokes transports (Chap. 2, Figs. 11 and 16-17)
- Barotropic streamfunction (Chap. 1, Fig. 4)
- SST (Chap. 2, Fig. 6)
- Surface heat and water fluxes (Chap. 2, Figs. 7-10)
- MOC streamfunction (Chap. 1, Figs. 5 and 7)
- Sea level (Chap. 1, Figs. 17-19)

2 Adiabatic Equilibrium of a Wind-Driven Zonal Jet

The cogent idealization of the ACC is an adiabatic, zonally periodic jet driven by a broad, steady zonal wind on the β-plane over irregular topography with a baroclinic deformation radius much

smaller than the wind and current scale (*i.e.,* $R \ll L_y$) and without surface buoyancy flux. The dynamics can be well represented by the QG approximation, and we will do so here. The problem configuration is shown in Fig. 1. Another important scale, which we can recognize as δ_c (Charney, 1955) for a nonlinear western boundary current, is $L_\beta = \sqrt{U/\beta}$, where U is a typical current velocity, either mean or eddy. In the ACC, $L_\beta < L_y$, though not necessarily by much; the implications of this are further commented on below.

First, consider spin-up from a stratified resting state. At early times the jet will accelerate with

$$u(y,z,t) \;\propto\; \tau_s^{(x)}(y)t\,, \tag{1}$$

where $\tau_s^{(x)} = u_*^2$ is the zonal wind stress divided by ρ_o. The early-time depth profile depends upon the scale of the wind forcing; when $L_\tau \gg R$, it is mostly barotropic (*i.e.,* depth independent).

To have any chance of arriving at an equilibrium state, the problem must be posed with non-conservative terms, *e.g.,* eddy viscosities ν_h and ν_v and/or bottom-drag damping rate ϵ_b. If these parameters are large enough, they can support a steady, stable jet in a late-time equilibrium. However, for smaller values, as geophysical plausibility requires, the accelerating jet will become unstable before it reaches a viscous steady state. A bifurcation sequence of successive instabilities can be mapped out, but geophysical jets are well past this transition regime; they can reach an equilibrium only in balance with fully developed geostrophic turbulence. The most important type of jet instability for $L > R$ is baroclinic instability.

Now consider the fully developed, statistical equilibrium state. Its instantaneous flow and potential vorticity in a numerical solution of the QG layered equations are shown in Fig. 5, and its buoyancy and vertical velocity are shown in Fig. 6. Note the strong, narrow, meandering jet near the surface, and the weaker, broader flow near the bottom. The centerline of the jet is a continuous front in temperature T, a broken front in potential vorticity q, and an axis of alternating centers in vertical velocity w.

We define an overbar as an average over (x,t), where the domain of each is taken to be infinite, consistent with our assumptions of zonal homogeneity and stationarity. The mean geostrophic flow is a surface intensified zonal jet, $\overline{u}(y,z) \equiv \overline{u}_m(y)$ (Figs. 2-3). This jet is in hydrostatic, geostrophic balance with the dynamic pressure $\overline{\phi}_m$, streamfunction $\overline{\psi}_m$, layer thickness $\overline{h}_m$, anomalous interfacial elevation $\overline{\eta}_{m+.5}$, and anomalous interfacial "temperature" $\overline{T}_{m+.5}$ (or, with a different notation for the layer interface index, $\overline{T}_\alpha$ with $\alpha = 1,\ldots,M-1$):

$$\begin{aligned}
u_m &= -\frac{1}{f}\frac{\partial \phi_m}{\partial y} \\
\psi_m &= \phi_m / f \\
h_m &= H_n + \eta_{m-.5} - \eta_{m+.5} \\
\eta_{m+.5} &= \frac{f}{g'_{m+.5}}(\psi_{m+1} - \psi_m) \\
T_{m+.5} &= -\frac{f}{\alpha g}(\psi_{m+1} - \psi_m)\,.
\end{aligned} \tag{2}$$

Here $g' = g\Delta\rho/\rho_0 = \Delta\overline{b}$ measures the effective stratification across an interface, and we have assumed the simple, equation of state, $\rho = -\alpha_T T \rho_0$ with α_T the thermal expansion coefficient.

The time-mean profiles from the same numerical solution are shown in Fig. 7. They show a surface intensified eastward jet; geostrophically balancing temperature gradients (with cold water on the poleward side of the jet); opposing potential vorticity gradients in the top and bottom layers (*i.e.,* satisfying a Rayleigh necessary condition for baroclinic instability) and homogenized q in the middle layer (*cf.,* Chap. 3, Sec. 3.5); and a mean upwelling on the poleward side of the jet and downwelling on the equatorward side (*i.e.,* a Deacon cell of an overturning secondary circulation in the meridional plane, whose surface branch of equatorward flow is the Ekman transport).

2.1 Zonal Momentum Balance

What is the zonal momentum balance for this state? Its most important part is

$$\frac{\partial \overline{u}}{\partial t} \; (=0) \; \approx \; \frac{\partial \tau}{\partial z} \, , \tag{3}$$

where

$$\begin{aligned} \tau &= \tau_s^{(x)}, \quad z = H \\ &= D, \quad b < z < H \\ &= D_b + \epsilon_b \overline{u}_b, \quad z = b \approx 0 \, , \end{aligned} \tag{4}$$

and we have assumed an Ekman layer form for the turbulent bottom drag. In a vertical integral of (4),

$$\frac{\partial}{\partial t} \int_b^H \overline{u} \, dz \; (=0) \; = \; W^{(x)} - [D_b + \epsilon_b \overline{u}_b] \, . \tag{5}$$

Thus, for $\tau^{(x)} > 0$, we need $\overline{u}_b > 0$ and/or $D_b > 0$. The latter, which is *topographic form stress*, dominates in the Antarctic Circumpolar current (Treguier and McWilliams, 1990; Wolff et al., 1991). Without topographic stress, the turbulent drag over a flat bottom is so inefficient with realistic values of ϵ_b that an unnaturally large bottom velocity and zonal transport is required to reach equilibrium, *e.g.,* in the zonal momentum balance.

For balance in (3) near the top and bottom surfaces, we also need $D > 0$; generally, $D > 0 \forall z$. D is the isopycnal form stress discussed in Chap. 3, Sec. 3.2, *viz.,*

$$D^{(x)} \; = \; -\overline{\phi_x \eta} \; = \; -f \overline{v \eta} \, . \tag{6}$$

In a momentum budget, like (3), we have

$$\begin{aligned} \frac{\partial u}{\partial t} &= \frac{\partial D^{(x)}}{\partial z}, \\ \frac{\partial u^{above}}{\partial t} &\sim -D^{(x)}/H^{above} \\ \frac{\partial u^{below}}{\partial t} &\sim +D^{(x)}/H^{below}\,. \end{aligned} \tag{7}$$

When the material surface is the bottom, then $\eta = B$ and

$$D_b = -f\overline{vB}\,. \tag{8}$$

Note that $D_b \neq 0$ requires that the time-mean $v \neq 0$; *i.e.,* there must be "standing eddies" present. When η is an isopycnal surface, we can derive

$$D_{m+.5} \;=\; -\frac{f}{g'_{m+.5}}\overline{v_m \psi_{m+1}}\,, \tag{9}$$

where the "turbulent" eddies can be either standing or transient.

To complete the characterization of the zonal momentum balance (*i.e.,* going beyond the approximation in (3)), we must also consider the horizontal Reynolds stress:

$$\frac{\partial \overline{u}}{\partial t}\;(=0) \;=\; \frac{\partial \tau}{\partial z} + \frac{\partial R}{\partial y} + \mathcal{O}(Ro,\, Re_h)\,, \tag{10}$$

where $R \equiv -\overline{uv}$. Thus, in each interior layer, the mean zonal flow is accelerated by the difference between the isopycnal form stress, $D(z)$, at the interfaces (isopycnal surfaces) above and below, and it is decelerated by the divergence of the horizontal Reynolds stress.

The time- and zonal-mean zonal momentum balance from the same numerical solution is shown in Fig. 8. In the upper layer, we see the eastward surface wind stress balanced primarily by eddy isopycnal form stress (*i.e.,* associated with the first interior interface between layers, $-D_1$), with the eddy horizontal Reynolds stress divergence redistributing momentum in y, increasing the eastward momentum in the core of the jet and decreasing it at the edges (a.k.a. negative eddy viscosity). In the bottom layer, we see eastward momentum transmitted downward by the isopycnal from stress (*i.e.,* $+D_2$) and balanced almost entirely by bottom stress, here represented by a bulk formula for drag by bottom boundary-layer turbulence, $-C_D|\mathbf{u}|u$, with negligible deep eddy horizontal Reynolds stress. These eddy momentum flux patterns are typical of broad baroclinically unstable zonal jets (*cf.,* the atmospheric westerly winds).

The most striking feature of R is the acceleration of the mean zonal jet in its meridional/vertical core. Eddy acceleration of the mean flow is referred to as a negative-viscosity behavior since it implies that the eddy Reynolds stress profile has the same shape in y as the mean horizontal shear. An explanation for R having this shape can be either made in terms of radiating Rossby waves (Sec.

2.4) or as a property of the linearly unstable eigenmodes for $\overline{u}_n(y)$. When $L_\tau > L_\beta > R$, multiple jets can occur, with a meridional scale near L_β (Panetta, 1993; Treguier and Panetta, 1994). The common view of the ACC, based on shipboard hydrographic transects and instantaneous altimetric fields, is that it typically has several cores of relatively intense narrow zonal flow embedded in the broader zonal of the ACC as a whole; it remains somewhat uncertain whether the same is true of the time-mean ACC.

2.2 Meridional Overturing Circulation (MOC)

The mean circulation is $(\overline{u}, \overline{v}, \overline{w})$, where only the zonal component is in geostrophic balance. The components in the meridional plane — the Deacon Cell — are ageostrophic velocities, and thus weaker by $\mathcal{O}(Ro)$.

Consider the relation expressing the movement of the interfaces as material surfaces,

$$w \;=\; \frac{D\eta}{Dt}. \tag{11}$$

The mean of this relation is

$$\overline{w} \;=\; \overline{u\eta_x} + \overline{v\eta_y} \;=\; \frac{\partial}{\partial y}\overline{v\eta} \;=\; -\,\frac{1}{f}\frac{\partial}{\partial y}D\,. \tag{12}$$

Thus, $\overline{w}$ is forced by the isopycnal form stress in the interior. By continuity,

$$\overline{v}_y + \overline{w}_z = 0\,, \;\; \text{or} \tag{13}$$

$$\overline{v} \;=\; \frac{1}{f}\frac{\partial}{\partial z}D \;\rightarrow\; \frac{D_{m-.5} - D_{m+.5}}{fH_m}\,. \tag{14}$$

When we combine (12) and (14) with the assumption that the PBL lies entirely within the upper layer of our model configuration, *i.e.,* that

$$\overline{w} \;=\; w_{ekman} \;=\; -\,\frac{1}{f}\frac{\partial}{\partial y}\tau_s^{(x)} \;\; \text{at} \;\; z = H\,, \tag{15}$$

then we obtain the clockwise mean meridional circulation seen in Fig. 4.

We can reinterpret (14), using the definition of h_m in (2), to express the condition that there can be no equilibrium flux of mass within any layer; *viz.,*

$$\overline{hv} \;=\; H\overline{v} + \overline{(h-H)v} \;=\; 0\,. \tag{16}$$

Thus, there is an exact cancellation of the mean mass flux within an isopycnal layer by the eddy mass transport. The same conclusion could be drawn for any non-diffusing tracer that does not cross the material interfaces. There can be no net flux of any material property in an adiabatic equilibrium state.

2.3 Meridional Heat Balance

D plays an essential role in the equilibrium balances for the jet. Where does it come from? From (2) we can write the interfacial temperature as $T = -g'\eta/\alpha g$. Hence, isopycnal form stress (6) can be related to lateral heat flux by

$$D = \frac{\alpha f g}{g'}\overline{vT}\,. \tag{17}$$

$D > 0$ implies $\overline{vT} < 0$, and, as can be seen from the shape of $\overline{T_{m+.5}}(y)$ in the figure above, this sign for D implies both a down-gradient heat flux and a release of available potential energy — as also found in the linear eigenmodes for baroclinic instability of $\overline{u}(y,z)$.

The equilibrium heat balance is

$$\overline{T}_t \ (=0) \ = \ -\frac{\partial}{\partial y}\overline{vT} - \overline{w}\overline{T}_z\,, \tag{18}$$

which is assured by the previous relations. Thus, there is no net heat flux and the eddies balance the mean ageostrophic advection exactly.

2.4 Rectification by Rossby Wave Radiation

A type of rectification that does not necessarily involve circulation instability arises when waves radiate away from a localized source region and decay in amplitude as they propagate. This effect can be illustrated for Rossby waves in solutions of the barotropic potential vorticity equation on the β-plane,

$$\begin{aligned} \frac{Dq}{Dt} &= F - r\zeta \\ q &= \nabla^2\psi + \beta y \\ \frac{D}{Dt} &= \frac{\partial}{\partial t} + \hat{\mathbf{z}}\cdot\boldsymbol{\nabla}\psi\times\boldsymbol{\nabla}, \end{aligned} \tag{19}$$

where the potential vorticity is $q = f + \zeta$; the vertical component of vorticity is ζ; the Coriolis frequency is $f = f_0 + \beta y$; F is a forcing term (*e.g.,* Ekman pumping due to the wind); and r is a damping coefficient (*e.g.,* Ekman drag). Consider the situation where $F = F_*(x,y)\sin[\omega t]$ and F_* is nonzero only in a narrow region in y (Fig. 9).

Rossby waves with frequency ω will be excited and propagate away from the source region. Their dispersion relation is

$$\omega = -\frac{\beta k}{k^2+\ell^2}, \tag{20}$$

where (k, ℓ) is the horizontal wavenumber vector. The associated meridional phase and group speeds are

$$\begin{aligned} c_p^{(y)} &= \omega/\ell = -\frac{\beta k}{\ell(k^2+\ell^2)} \\ c_g^{(y)} &= \frac{\partial \omega}{\partial \ell} = \frac{2\beta k \ell}{(k^2+\ell^2)^2}\,. \end{aligned} \tag{21}$$

To the north of the source region, the group speed must be positive for outward energy radiation. Without loss of generality we can choose $k > 0$; hence the northern waves must have $\ell > 0$ for northward radiation. This implies $c_p^{(y)} < 0$ and a NW-SE alignment of the constant-phase lines, hence $\overline{u'v'} < 0$ since the horizontal velocity is parallel to the constant-phase lines. In the south the constant-phase lines have a NE-SW alignment, and $\overline{u'v'} > 0$. This leads to the $\overline{u'v'}(y)$ profile in Fig. 9. Notice the amplitude decay as $|y| \to \infty$, due to damping by r. In the vicinity of the source region the flow can be complicated, depending upon the form of F_*, and here we simply connect the far-field relations smoothly across it without being too concerned about local details.

This horizontal Reynolds stress enters in the time-mean, zonal momentum balance as

$$r\overline{u} = -\frac{\partial}{\partial y}\left(\overline{u'v'}\right) \tag{22}$$

since $\overline{F} = 0$. Thus the mean zonal flow generated by wave rectification has the pattern sketched in Fig. 9, eastward in the vicinity of the source and westward to the north and south. This a simple model for the known behavior of eastward acceleration by the eddies in an baroclinically unstable eastward jet (*e.g.,* in the Jet Stream and ACC), where the eddy generation process by instability has been replaced in this simple mechanistic model by the transient forcing F. Note that this rectification does not act like an normal eddy mixing process in the generation region since

$$\nu_e \equiv -\frac{\overline{u'v'}}{\overline{u}_y} < 0\,, \tag{23}$$

although this ratio is positive in the far field. The reason is that the eddy process is highly non-local, with the eddy generation site distant from the dissipation site. Associating westard momentum with Rossby waves, we can say that they receive westard momentum from (or impart eastward momentum to) the mean flow where they are generated and deposit or impart westard momentum to the mean flow where they are dissipated. Since

$$\int_{-\infty}^{\infty} \overline{u}(y)\, dy = 0 \tag{24}$$

from (22), we can view the rectification process as a conservative redistribution of the ambient mean zonal momentum – initially zero everywhere and integrally zero at all times — through Rossby-wave radiation stresses.

There are other important examples of non-local transport of momentum by waves, taking it from where they are generated and depositing it where they are dissipated. This is what happens for

gravity lee waves generated by flow over topography, propagating upward and breaking at critical levels where they then retard the mean flow (*e.g.,* certainly in the tropopause jet stream or perhaps in the upper part of the ACC too).

2.5 Alternative Languages for Theoretical Interpretation

Much of what is presented above is a picture that was first drawn in the 1950s and 1960s to describe the maintenance of the atmospheric jet stream (*e.g.,* Lorenz (1967)), even though for many years afterwards it was still a serious challenge to realize computational solutions for this behavior. The ACC and jet stream have a lot in common. Perhaps the biggest difference being is that the former is driven by a mean surface stress and the latter by a mean meridional heating gradient, and the associated vertical wind shears and meridional temperature gradients are related by thermal wind. This GFD problem is such an important one that its interpretation has continually been developed further. A variety of languages have been developed in this context:

- Eulerian mean circulation: $(\overline{u}, \overline{v}, \overline{w})$.
- Eliassen-Palm (EP) flux: $\vec{F} \ = \ (0, R, D)$.
- Residual-mean circulation: $(0, \overline{\tilde{v}}, \overline{\tilde{w}})$, where

$$\overline{\tilde{v}} = \overline{v} - \frac{1}{f} D_z, \ \ \overline{\tilde{w}} = \overline{w} + \frac{1}{f} D_y \, . \tag{25}$$

  The final r.h.s. terms are the non-divergent *eddy-induced transport velocity*, $\mathbf{u}^*$, that appears in the widely used eddy tracer transport parameterization of Gent and McWilliams (1990), discussed in Chap. 3, Sec. 3.3. (Residual-mean flow may be defined more operationally as the Lagrangian mean flow for passive tracers, *i.e.,* the net motion due to the Eulerian mean flow and the eddy-induced Largrangian transport.)

- Transformed Eulerian Mean (TEM) equations: for an average that is now made in x, a diabatic fluid, and quasigeostrophic relations [with a harmless extra $\mathcal{O}(Ro)$ meridional advection in the temperature equation], we can write a transformed dynamical set of equations for the Eulerian mean zonal flow, $\overline{u}(y, z, t)$:

$$\begin{aligned} \overline{u}_t - f\overline{\tilde{v}} &= \vec{\nabla} \cdot \vec{F} + n.c.t. \\ \overline{T}_t + \overline{\tilde{v}}\overline{T}_y + \overline{\tilde{w}}\overline{T}_z &= n.c.t. \\ \overline{\tilde{v}}_y + \overline{\tilde{w}}_z &= 0 \\ f\overline{u}_z + \alpha g \overline{T}_y &= 0 \, . \end{aligned} \tag{26}$$

  In these equations $n.c.t.$ denotes any non-conservative terms in zonal momentum and heat. These equations have subtracted the geostrophic balance terms from the zonal momentum

equation, and all the eddy effects appear explicitly only in one place as the EP flux divergence. The residual-mean flow acts as the effective transport velocity for passive tracers as well as buoyancy/temperature, although for tracers there are additional eddy flux terms for lateral mixing along isopycnal surfaces (*n.b.,* mixing buoyancy along an isopycnal surface has no effect).

- Eddy potential vorticity flux:

$$\overline{v'q'} \;=\; R_y + D_z \;=\; \vec{\nabla}\cdot\vec{F}\,, \tag{27}$$

using the definition for potential vorticity, $q' \;=\; v'_x - u'_y - f_0\eta'_z$. This the eddy forcing term that appears in the TEM zonal momentum balance.

- Adiabatic equilibrium: the relations (12)-(14) imply

$$\overline{\tilde{v}} = \overline{\tilde{w}} = 0 \quad \text{and} \quad \vec{\nabla}\cdot\vec{F} = -n.c.t.\,,$$

where the latter consist of the surface wind stress, bottom drag, and interior momentum diffusion.

- Non-acceleration, non-interaction, and Eliassen-Palm theorems (Andrews et al., 1987): in adiabatic equilibrium and with $n.c.t. = 0$, there are no eddy rectification effects on the zonal mean flow.

Now consider the behavior implied by the GM parameterization of geostrophic turbulence and its effects on the mean circulation. This parameterization addresses the isopycnal form stress but not the horizontal Reynolds stress (*i.e.,* D not R; Chap. 3, Sec. 3.2). If the interior of the ocean is approximately in adiabatic equilibrium, steady time, and without important $n.c.t.$ effects on the mean circulation, then the residual-mean circulation will be zero and a non-acceleration state will occur. Evidently these conditions are approximately realized in a coarse-resolution OGCM using the GM parameterization in Fig. 10, where the eddy-induced circulation nearly cancels the Eulerian-mean Deacon cell, except very near the surface (*i.e.,* in the vicinity of the diabatic PBL). An alternative parameterization of the rectified, mesoscale-eddy, tracer transport as horizontal eddy diffusion of buoyancy and tracers (the historically common practice) leads to a very different outcome. The implications for material property fluxes across the ACC are significant, such that the net flux (mean advection plus eddy rectification) is much smaller than the flux caused only by the mean Eulerian circulation (but also see Sec. 3).

In summary, we see the pervasive dynamical importance of form stress, both isopycnal, D, and topographic, D_{-H}, in extra-tropical, nearly adiabatic, wind-driven circulations. The spatial structure of the form stress is particularly simple in the zonally periodic ACC, which is therefore an easier context for understanding it. In 3D, baroclinic wind gyres, form stress is also important (*e.g.,* in resolving the dilemma of surface confinement; Chap. 3, Sec. 3.1), but its spatial structure is much more complex and its degree of dominance over horizontal Reynolds stress is less extreme (because the strong boundary currents are not broad compared to the deformation radius, R).

3 Coupling to the Thermohaline Circulation

The idealized model in Sec. 2 does not include effects of surface buoyancy flux and diabatic interior mixing. The common opinion is that these are of secondary influence on the ACC, but there are several reasons why this might not be true. First we discuss one associated with bottom topography. Figure 11 shows the barotropic streamfunction from three global GCM solutions presented in Cai and Baines (1996). They have surface buoyancy forcing (specified by restoring toward the climatological surface values of T and S) but no wind forcing. They differ only in their bottom topography: flat (run F1l I), a small ridge obstructing the Drake Passage south of South America (run F1I1p), and a larger ridge there (run F1Ipp). In all cases there is a thermohaline circulation in response to the buoyancy forcing (Chap. 6), but this has little expression in the depth-avveraged (barotropic) transport. In the first case there is essentially no barotropic transport anywhere, including in the ACC. This is consistent with Sverdrup theory and the adiabatic, wind-driven problems in Chap. 3 and Sec. 2. However, with a topographic ridge, a substantial eastward transport develops in the ACC.

This, too, can be interpreted as a consequence of topographic form stress, except that here $D_{-H} < 0$ is acting in (5) to accelerate the ACC, instead of decelerating it as in the usual wind-driven situation. The cause is the formation of dense water in the Weddell Sea that flows northward along the eastern side of the ridge in the Drake Passage. Denser water to the east of the ridge implies a larger bottom pressure there:

1. The pressure anomaly in the fluid decreases further to the east, so that the northward flow on the ridge slope is in geostrophic balance (*i.e.,* $\phi_x < 0$ and $v = \phi_x/f > 0$ since $f < 0$).

2. The larger bottom pressure is on the eastern slope, where $B_x < 0$, with smaller pressure on the western slope, where $B_x > 0$. By first line in (8), this implies $D_{-H} < 0$.

So, it is possible to create an eastward ACC with only thermohaline forcing and topographic form stress. In Fig. 11, the transport through the Drake Passage with the largest ridge is 110 Sv; this is almost as large as the observed transport. On the other hand, in the same paper, other GCM solutions are reported with wind forcing in all combinations with and without buoyancy forcing and with and without bottom topography. Somewhat surprisingly, the ACC transport varied in these cases only within the range 120-131 Sv, indicating that similar transport magnitudes may be achieved by several different dynamical circumstances.

Second, there is continuing scientific debate over whether the global thermohaline circulation (THC) is "pulled" downwards by deep convection or "pushed" towards the sinking regions by northward Ekman transport in the ACC region (*i.e.,* the surface branch of the Deacon Cell; Toggweiler and Samuels (1998)). There is no question that pulling can drive the THC (Chap. 6), since it can be realized in models with no wind driving and no zonally periodic circumpolar latitude band. The question of whether it can be pushed is whether the northward surface drift will continue past

the ACC — going against the southward Ekman pumping in the Trade Wind zone — or sink and become a closed MOC in the ACC region (as it mostly does in Fig. 10). There is a related, though not identical, question about whether an unusually large amount of the rising branch of the THC ascends in the neighborhood of the ACC, rather than more broadly around the world as traditionally believed and as implied by the global conveyor-belt cartoon (Chap. 1, Fig. 7). Since the ACC region is atypically weakly stratified, the amount of diapycnal mixing required to balance upward advection is relatively smaller. I am not explaining any further about these issues, but I have appended a relevant recent article by Webb and Suginohara (2001).

Third, the surface fluxes of heat and water in the ACC region (Chap. 2, Figs. 7 and 9), although nowhere near global maxima in their strength are non-zero, and there must be at least some degree of buoyancy forcing for the ACC. This is perhaps most significant for the MOC, although even the zonal flow may be influenced by changes in the meridional T and S gradients due to buoyancy forcing and expressed through the thermal wind relation. The observed meridional fields are shown in Fig. 12, although it is impossible to say which aspects are wind- or buoyancy-driven. Other observational fields (and their interpretation for the MOC) are in Fig. 13. One means of inferring the MOC is by tracing the water mass properties, and sometimes this approach is formalized by so-called *inverse models* (Speer et al., 2000). Figure 14 shows estimates of the surface water mass transformation, and Fig. 15 shows a schematic pattern for the inferred MOC. Since material transport by the Eulerian-mean MOC is substantially opposed by eddy fluxes in a quasi-adiabatic conception of ACC dynamics (Sec. 2), water-mass tracking is primarily focused on the net Lagrangian transport. This transport is often idenitifed with the residual-mean circulation (Sec. 2.5; Marshall and Radko (2003)). An interesting aspect of the diabatic MOC in the ACC is that the northward surface Ekman current is in the direction of increasing T; hence, a water parcel must gain heat as it moves northward. Apart from implausible heat sources from below or a large lateral eddy diffusion effect, there must therefore be net atmospheric heating in a latitude range where the air-sea interaction implies strong cooling in the Northern Hemisphere. The climatological flux estimate (Chap. 2, Fig. 7) does not have a strong signal in the ACC region.

Appendix: Webb and Suginohara (2001) (next page)

Oceanography

Vertical mixing in the ocean

The thermohaline circulation of the ocean results primarily from downwelling at sites in the Nordic and Labrador Seas and upwelling throughout the rest of the ocean. The latter is often described as being due to breaking internal waves. Here we reconcile the difference between theoretical and observed estimates of vertical mixing in the deep ocean by presenting a revised view of the thermohaline circulation, which allows for additional upwelling in the Southern Ocean and the separation of the North Atlantic Deep Water cell from the Antarctic Bottom Water cell. The changes also mean that much less wind and tidal energy needs to be dissipated in the deep ocean than was originally thought.

Previous calculations of vertical mixing based on the stratification of the deep ocean[1,2] assumed that a flux of 25 or 30 sverdrups (Sv) of water, made up of both deep and bottom waters, is injected at depths of about 4,000 metres and mixed upwards to depths near 1,000 m by turbulent mixing. Both reports conclude that the spatially averaged diapycnal (cross-density surface) mixing coefficient is 10^{-4} m^2 s^{-1}.

However, observations of turbulence[3] and dye diffusion[4] in the deep ocean indicate that there exists a background diapycnal diffusivity of only 10^{-5} m^2 s^{-1}, although much larger values are found in localized regions near rough topography[5]. The background value is consistent with mixing due to the background internal wave field, and the larger values are consistent with extra internal waves due to the interaction of currents with topography.

But it is not obvious that the latter is enough to raise diffusivity by an order of magnitude when averaged over the whole ocean. The extra power required to do this is also large[6]. If the efficiency is 20%, which is normally considered a maximum for the final stage of breaking internal waves, then the power required is 2.1 terawatts. This is just possible, given current estimates of the energy input from the wind and tides, but this figure does not allow for losses at other stages in the conversion process.

A contrasting view of the thermohaline circulation has come from low-resolution[7] and high-resolution[8] computer model studies of the ocean circulation. These show that between 9 and 12 Sv of deep water is brought to the surface by Ekman suction in the Southern Ocean. This is driven northwards in the surface Ekman layer and is reduced in density primarily by surface freshening. The model results also emphasize earlier observations[9] that in the primary regions of bottom-water formation around Antarctica, the near-surface water masses have the same density as North Atlantic deep water. It is therefore not necessary for the bottom water to be mixed through the whole depth of the water column, only up to the level of the deep waters.

Using this new view of the thermohaline circulation, we need only consider the vertical mixing of the main deep-water mass, North Atlantic Deep Water, whose flux is estimated to lie between 14 and 17 Sv (ref. 10). Taking the larger of these two values and the smaller of the two model-based estimates of upwelling leaves a maximum of 8 Sv to be mixed vertically within the ocean. The 10^{-5} m^2 s^{-1} background term can upwell 3 Sv, leaving 5 Sv to be upwelled by localized regions of intense mixing. If this view is correct, then the vertical mixing coefficient, averaged over the whole ocean, is less than 3×10^{-5} m^2 s^{-1} and, assuming 20% efficiency, the total amount of extra energy required is less than 0.6 terawatts.

The revised values are consistent with existing observations of mixing within the ocean. They also emphasize again the importance of the Southern Ocean and imply that although further research is needed on the localized mixing in the deep ocean, such mixing does not control the thermohaline circulation.

D. J. Webb*, N. Suginohara†

**Southampton Oceanography Centre, Empress Dock, Southampton SO14 3ZH, UK*
e-mail: david.webb@soc.soton.ac.uk
†Center for Climate System Research, University of Tokyo, 4-6-1 Komaba, Meguro-ku, Tokyo 153-8904, Japan

1. Munk, W. H. *Deep-Sea Res.* **13,** 707–730 (1966).
2. Munk, W. H. & Wunsch, C. *Deep-Sea Res.* **45,** 1977–2010 (1998).
3. Gregg, M. C. *J. Geophys. Res.* **94,** 9686–9698 (1989).
4. Ledwell, J. R., Watson, A. J. & Law, C. S. *J. Geophys. Res.* **103,** 21499–21529 (1998).
5. Polzin, K. *et al. Science* **276,** 93–96 (1997).
6. Wunsch, C. *Nature* **405,** 743–744 (2000).
7. Toggweiler, J. R. & Samuels, B. *J. Phys. Oceanogr.* **28,** 1832–1852 (1998).
8. Döös, K. & Coward, A. C. *Int. WOCE Newslett.* **27,** 3–4 (1997).
9. Foster, T. D. & Carmack, E. C. *Deep-Sea Res.* **23,** 301–317 (1976).
10. Schmitz, W. J. *Rev. Geophys.* **33,** 151–173 (1995).

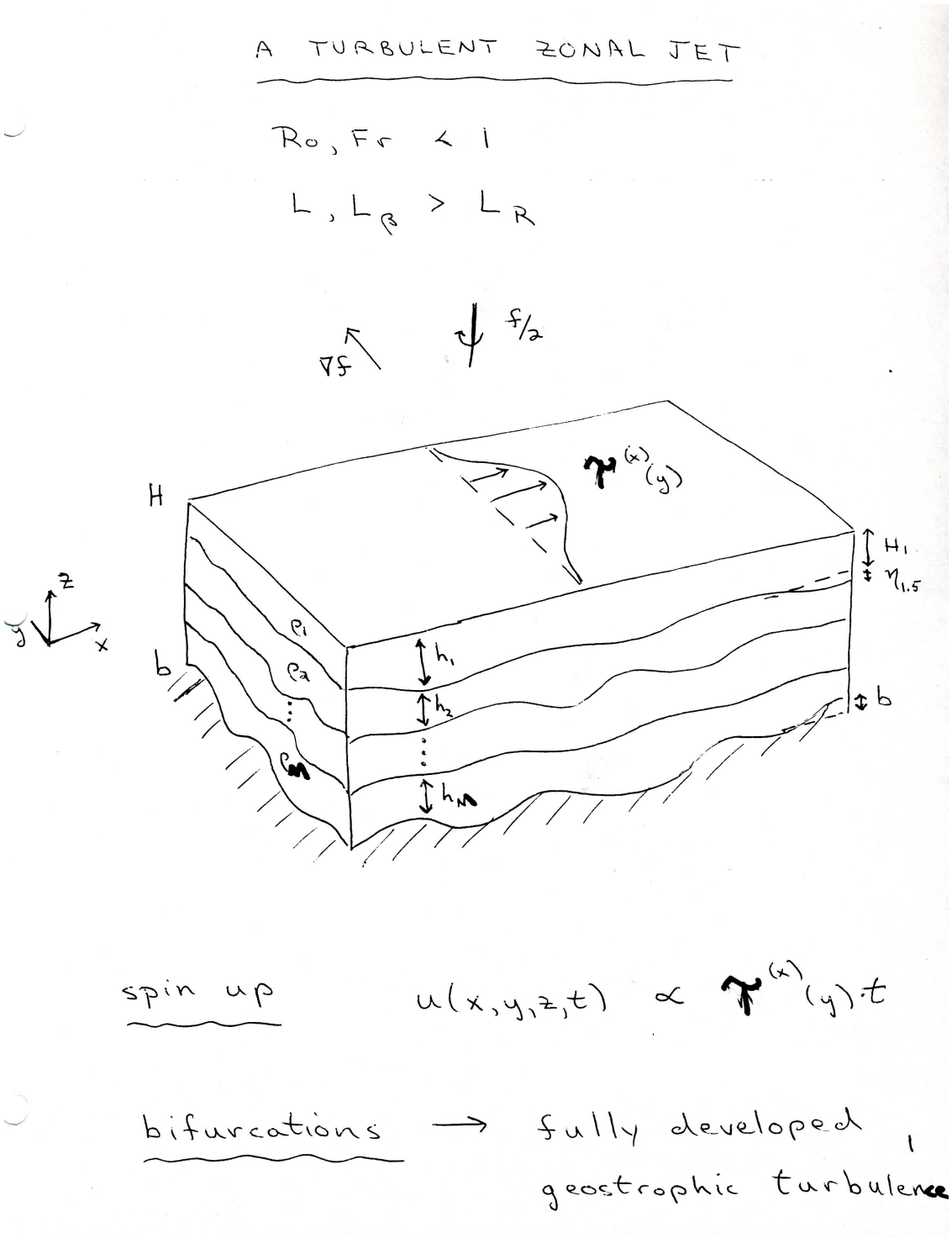

Figure 1: Posing the wind-driven zonal jet problem in the southern hemisphere.

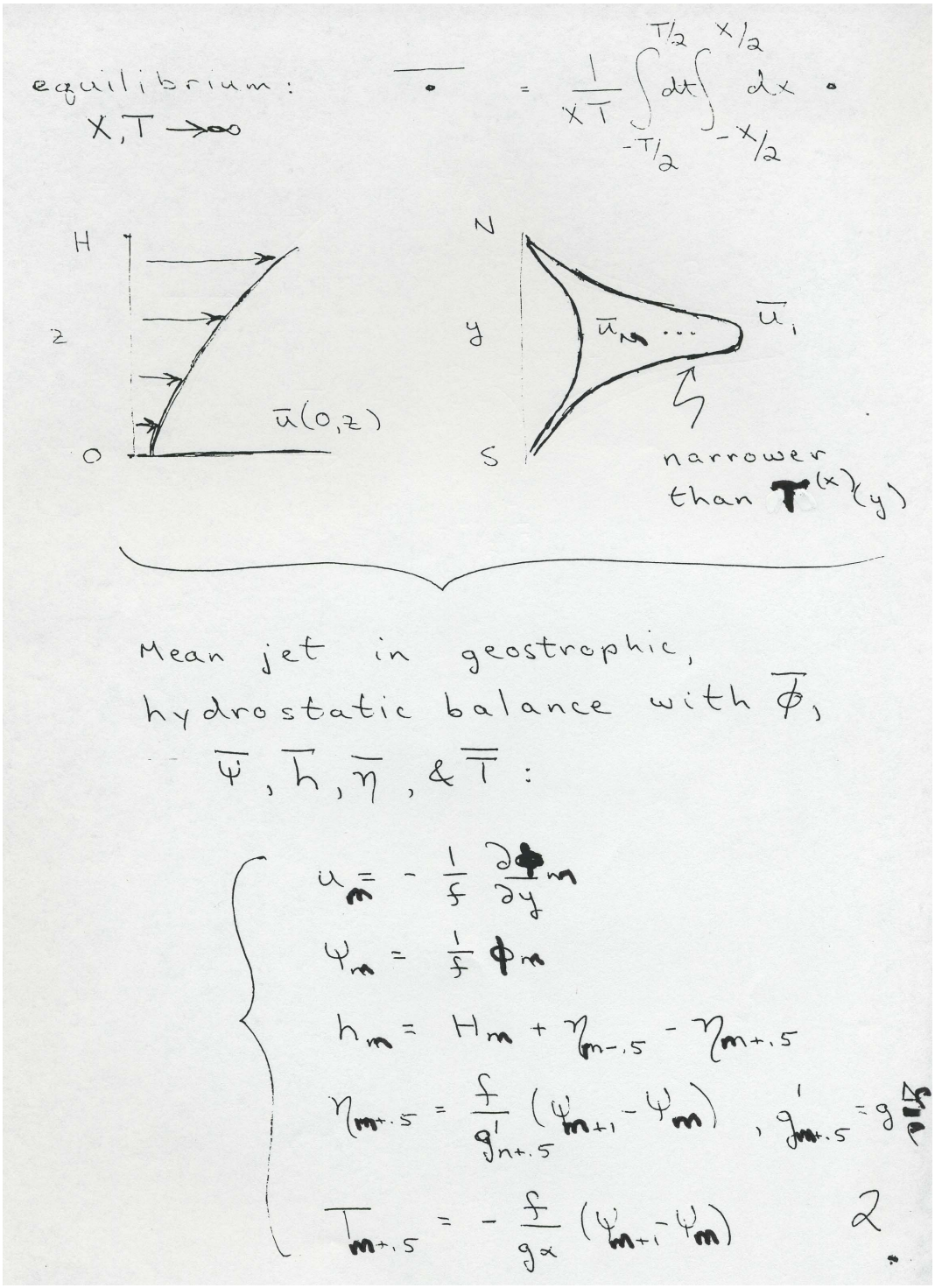

Figure 2: Sketch of the time-mean zonal flow in the zonal jet problem.

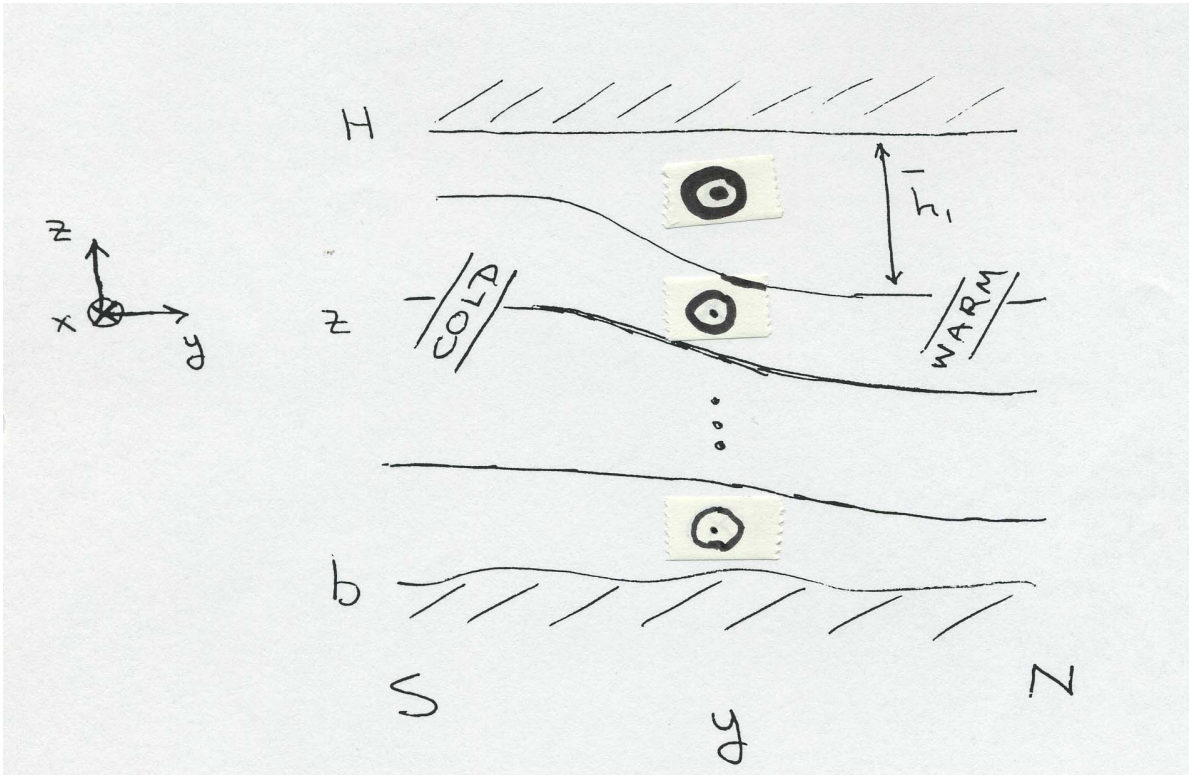

Figure 3: Sketch of a meridional cross-section for the time-mean zonal jet and buoyancy field.

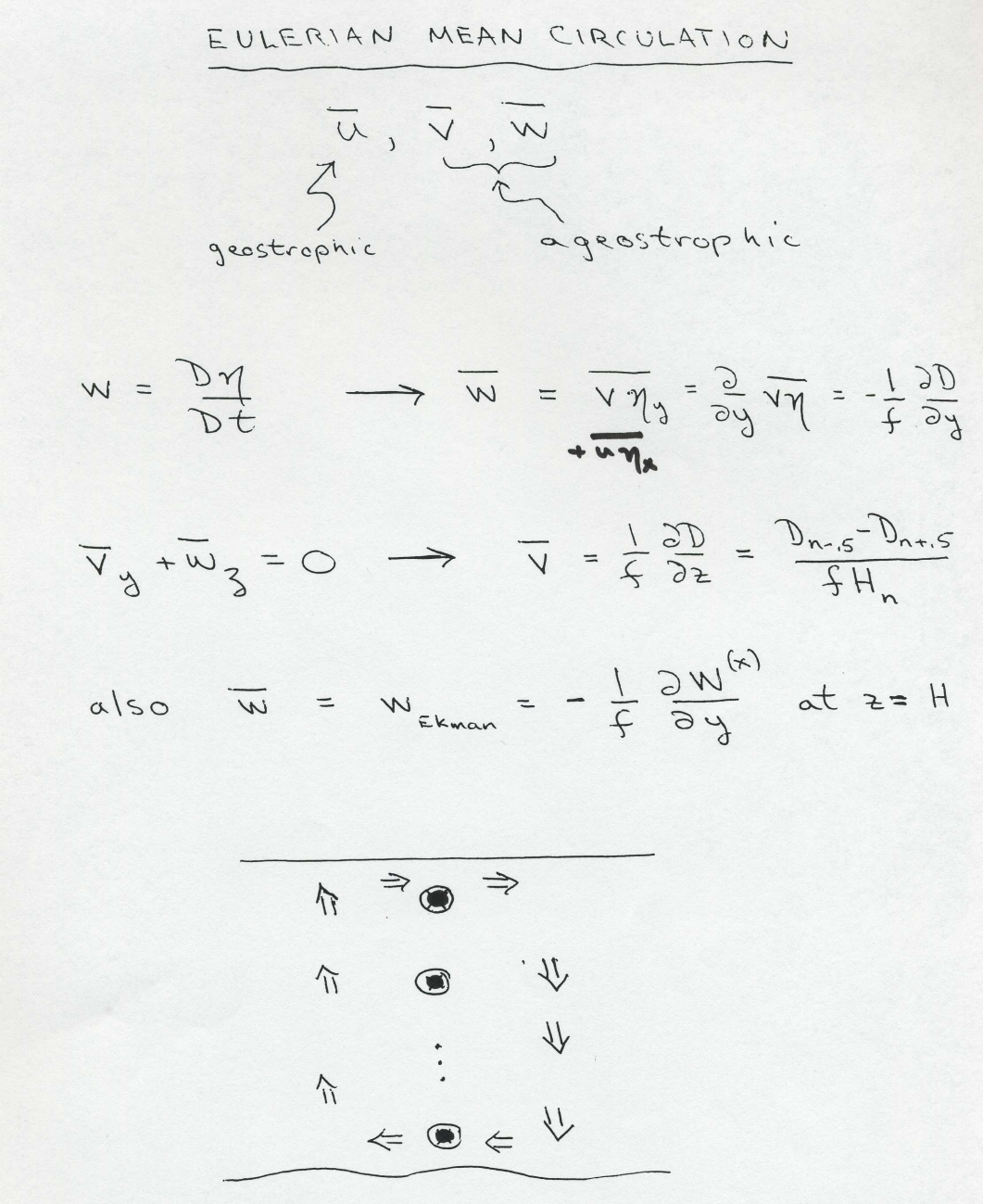

Figure 4: Sketch of the time-mean, meridional overturning circulation (*i.e.,* Deacon Cell) for the zonal jet.

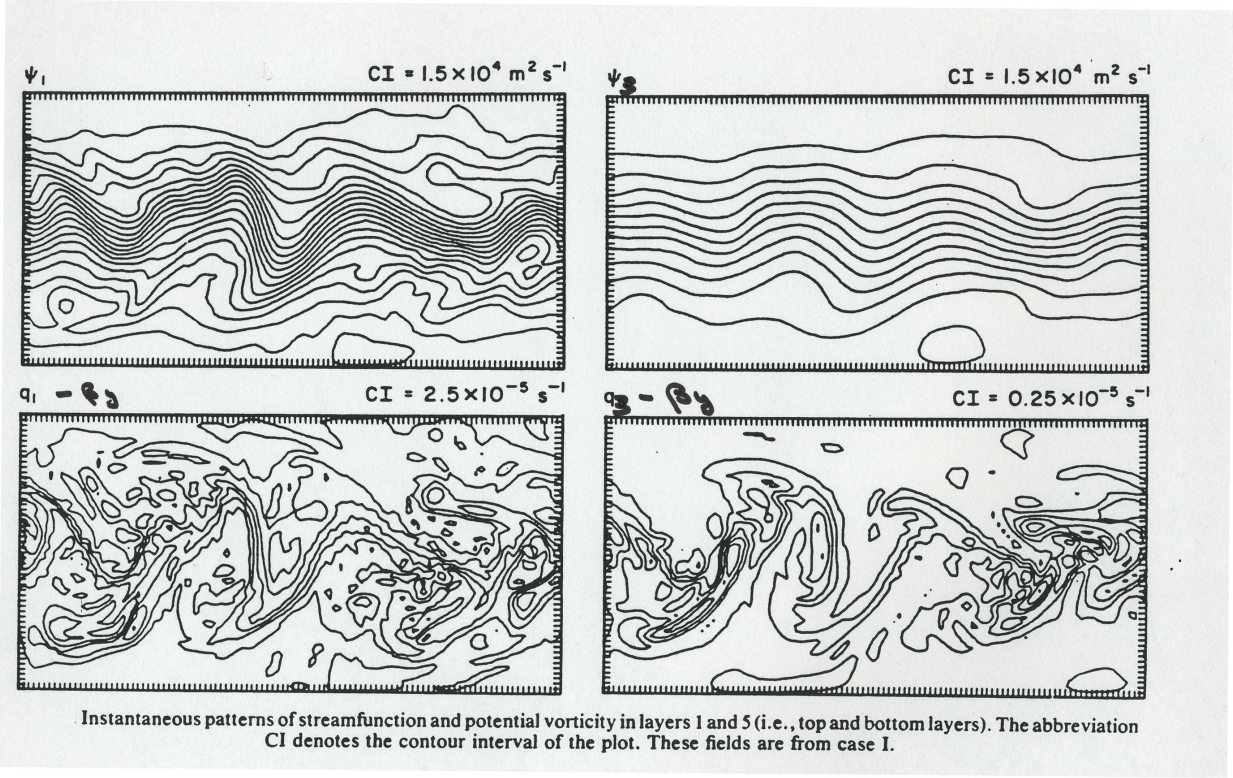

Instantaneous patterns of streamfunction and potential vorticity in layers 1 and 5 (i.e., top and bottom layers). The abbreviation CI denotes the contour interval of the plot. These fields are from case I.

Figure 5: Instantaneous streamfunction and potential vorticity (*i.e.,* excluding βy) patterns in the upper- and lower-most layers in a QG zonal-jet solution with $M = 3$ (McWilliams and Chow, 1981).

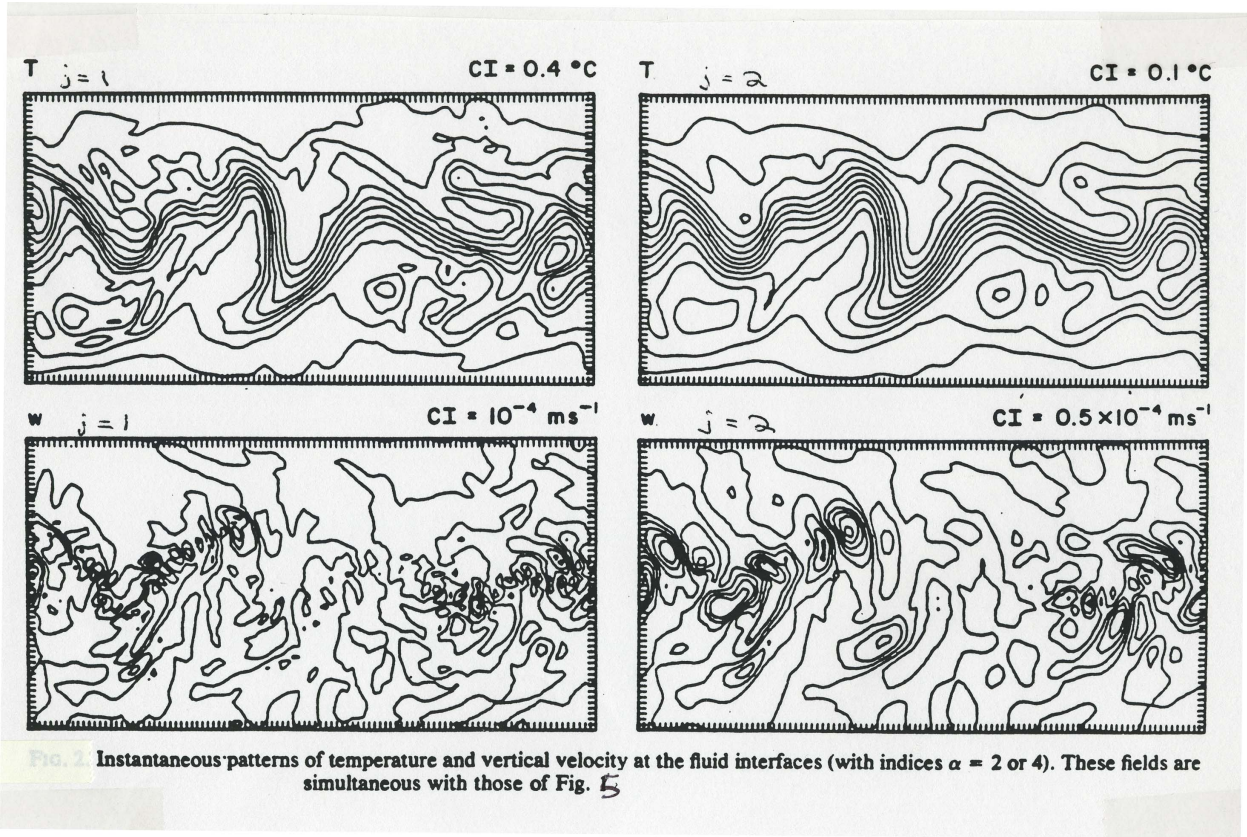

Figure 6: Instantaneous buoyancy and vertical velocity patterns at the the upper and lower interior interfaces in a QG zonal-jet solution with $M = 3$ (McWilliams and Chow, 1981).

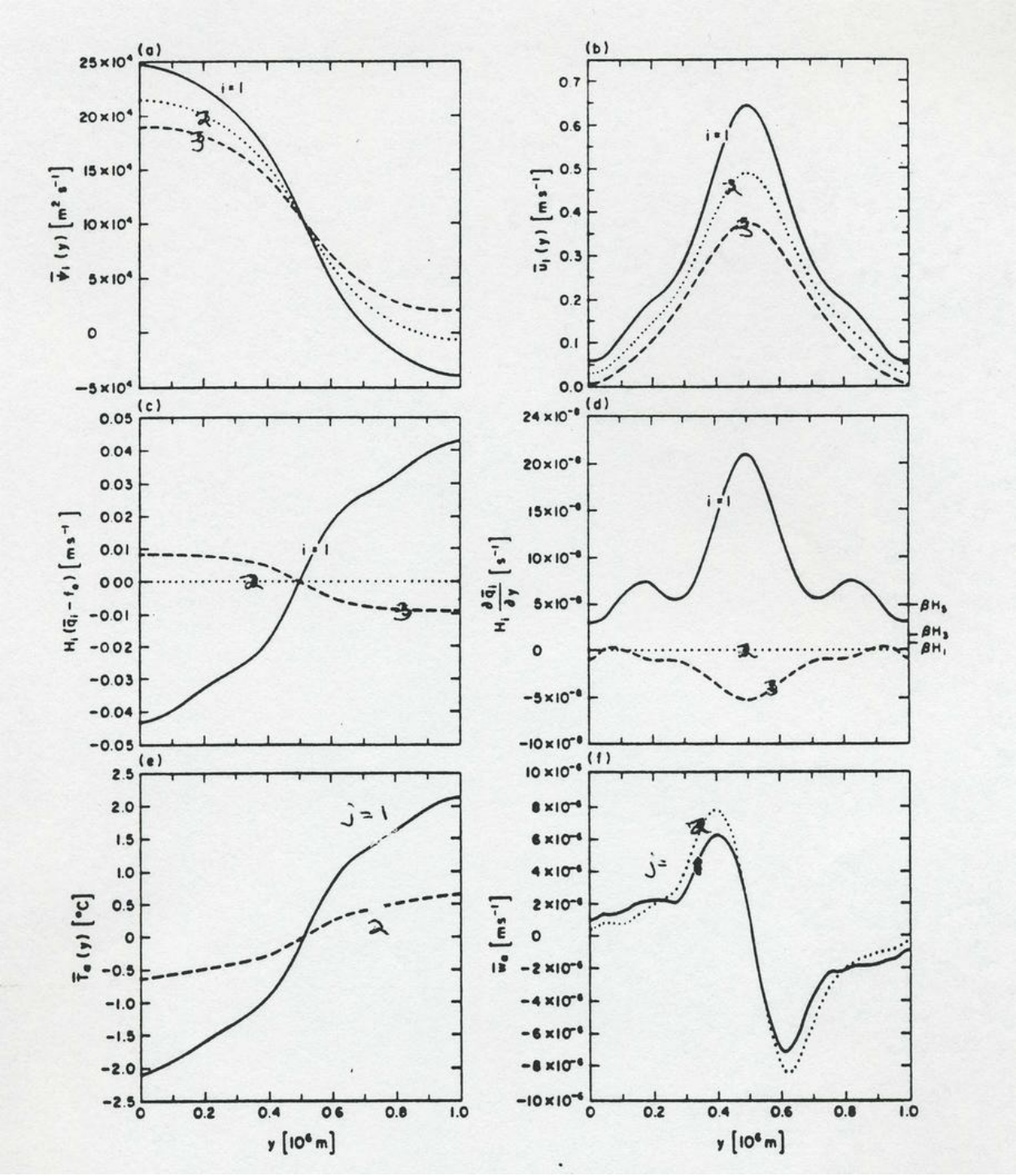

Figure 7: Time-mean meridional profiles for a QG zonal-jet solution with $M = 3$ (McWilliams and Chow, 1981): $\overline{\psi}_i,\ \overline{u}_i,\ H_i(\overline{q}_i - f_0),\ H_i\partial_y\overline{q}_i,\ \overline{T}_\alpha,\ \&\ \overline{w}_\alpha$.

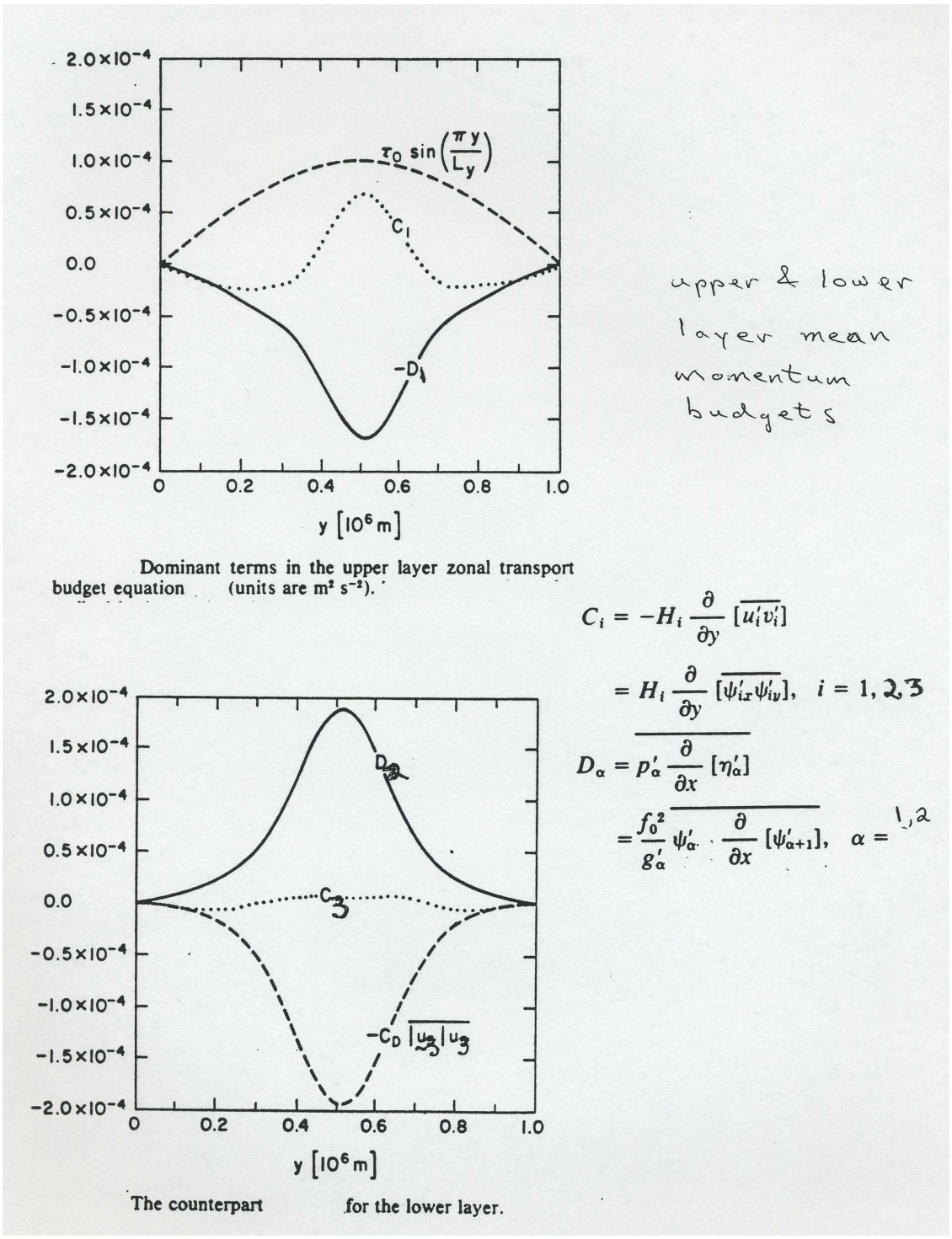

Figure 8: Terms in the zonal momentum budget in the upper- and lower-most layers for a QG zonal-jet solution with $M = 3$ (McWilliams and Chow, 1981).

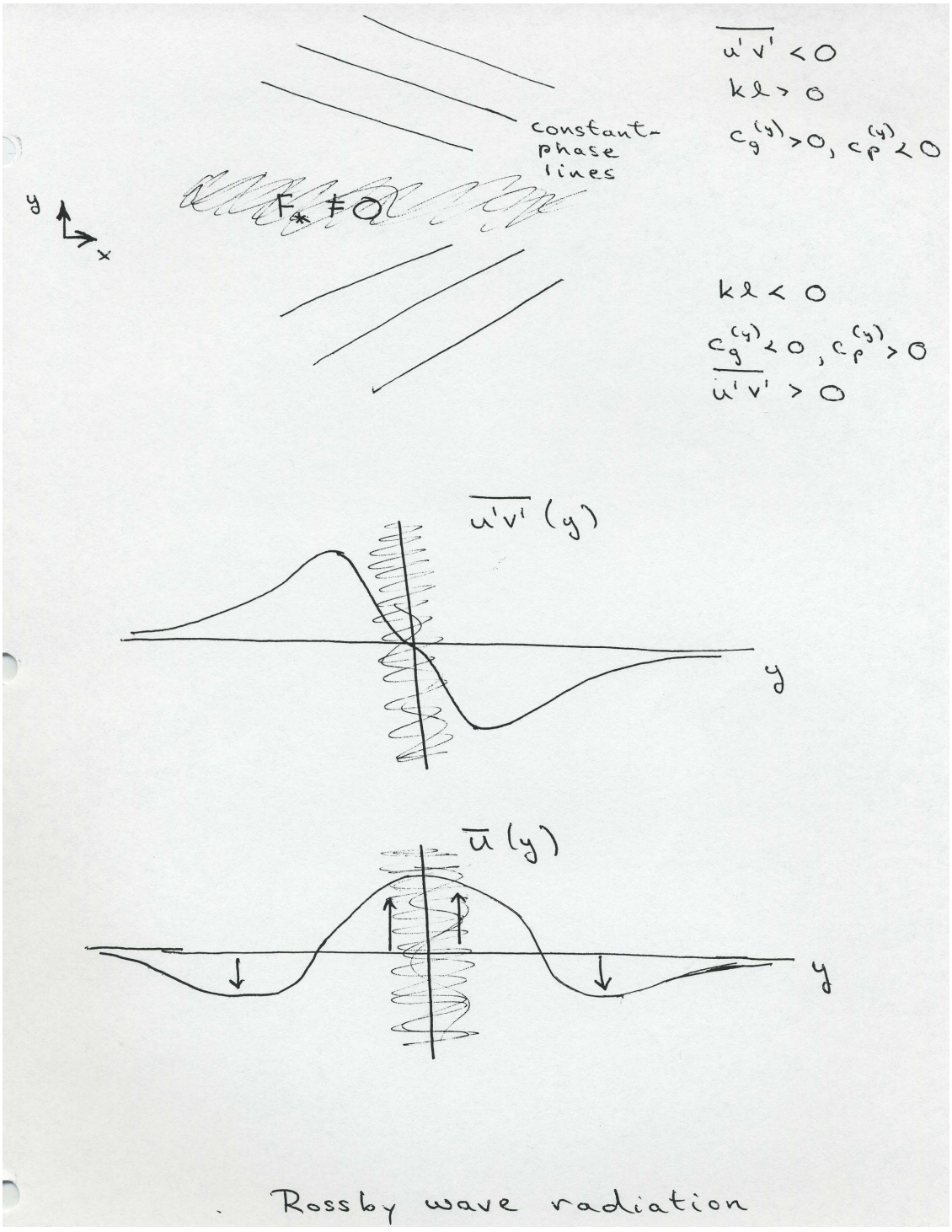

Figure 9: Sketch of radiating Rossby waves from a zonal line source and the resulting Reynolds stress and mean zonal flow.

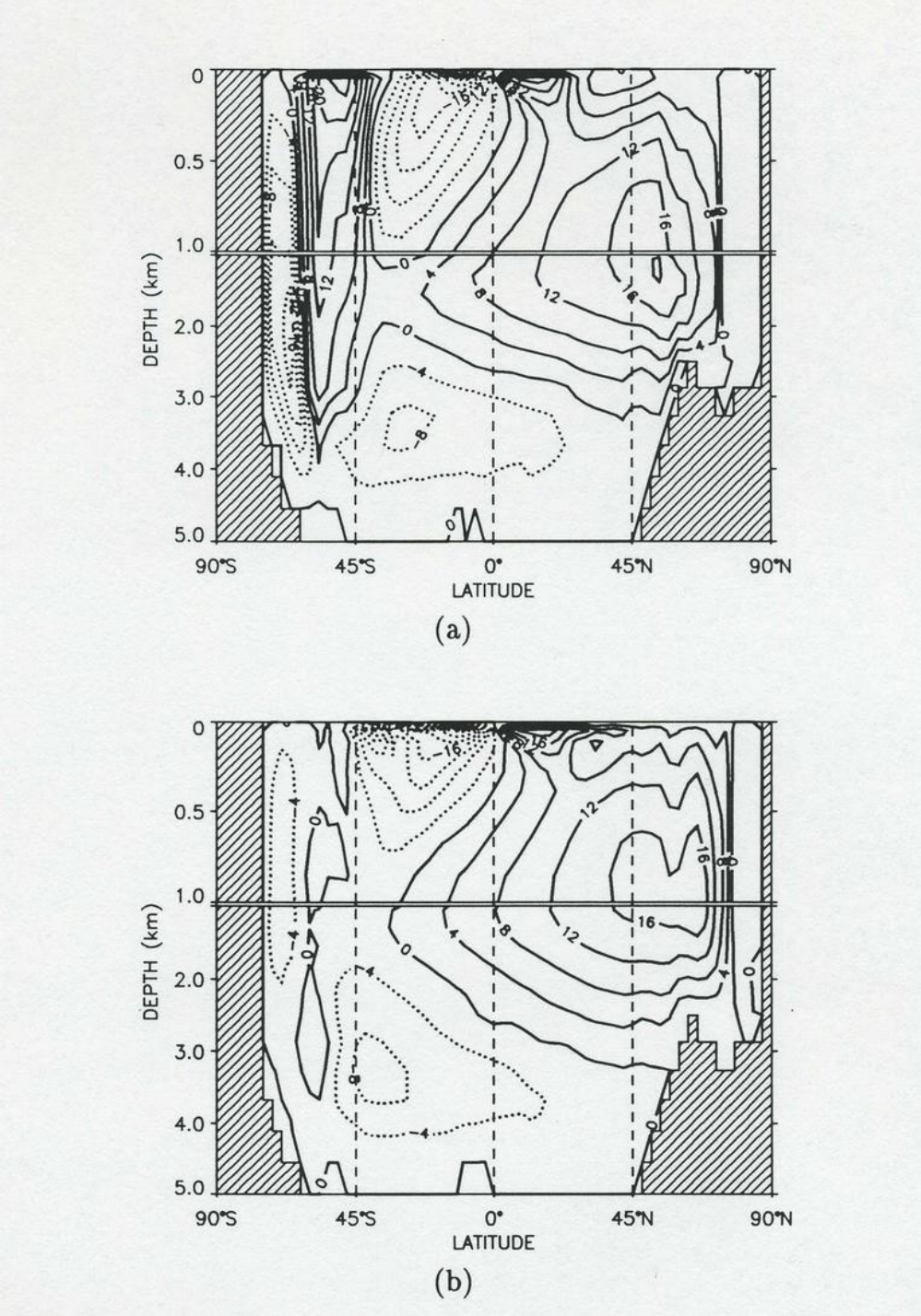

Figure 10: Time- and zonal-mean MOC Φ in the meridional plane from global equilibrium GCM solutions. HOR denotes a solution with κ_h as the mesoscale-eddy tracer diffusivity and ISO denotes one with κ_i as the isopycnal eddy-induced advection and mixing diffusivity (Danabasoglu and McWilliams, 1976).

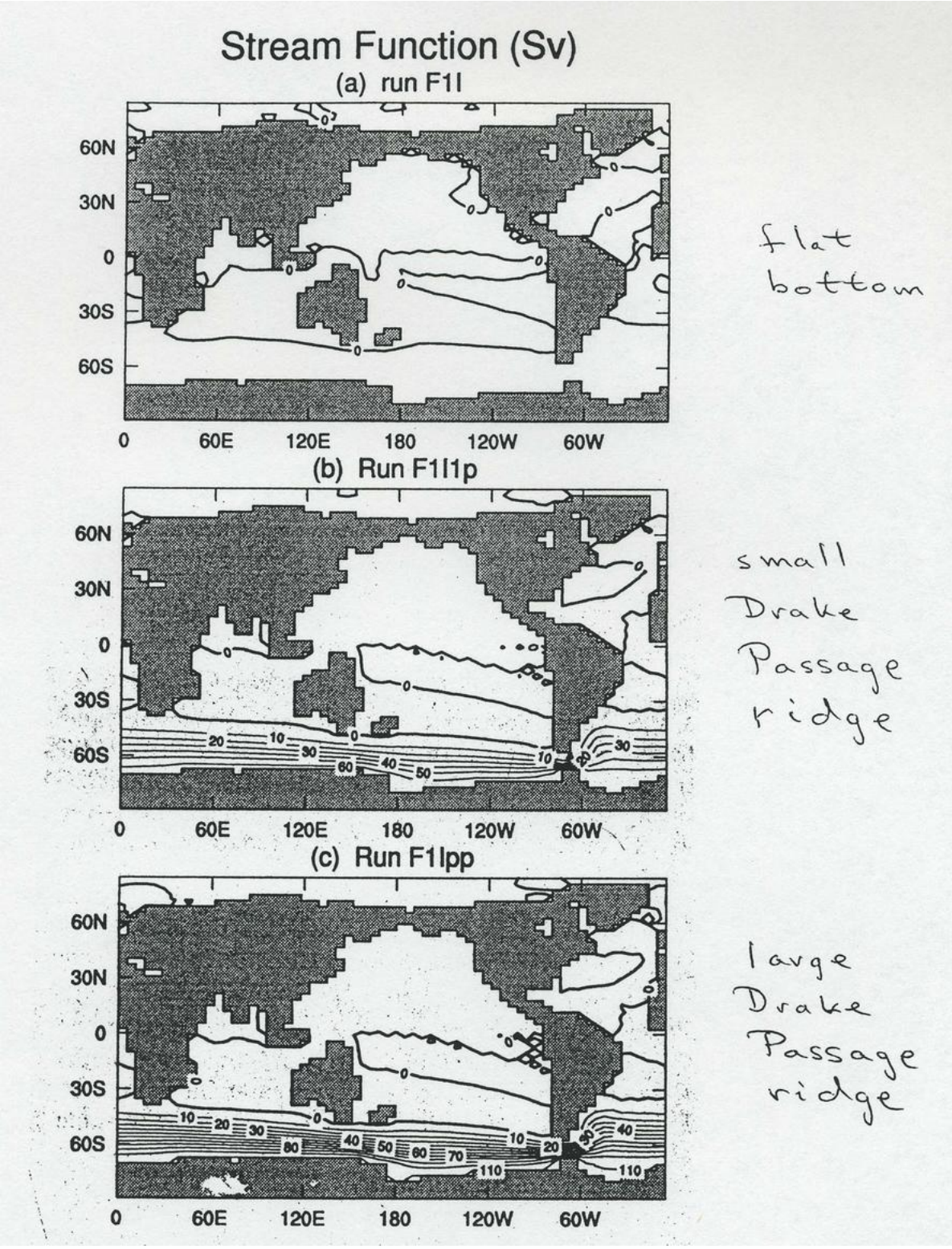

Figure 11: Thermohaline driving of the ACC through topographic torques (Cai and Baines, 1996).

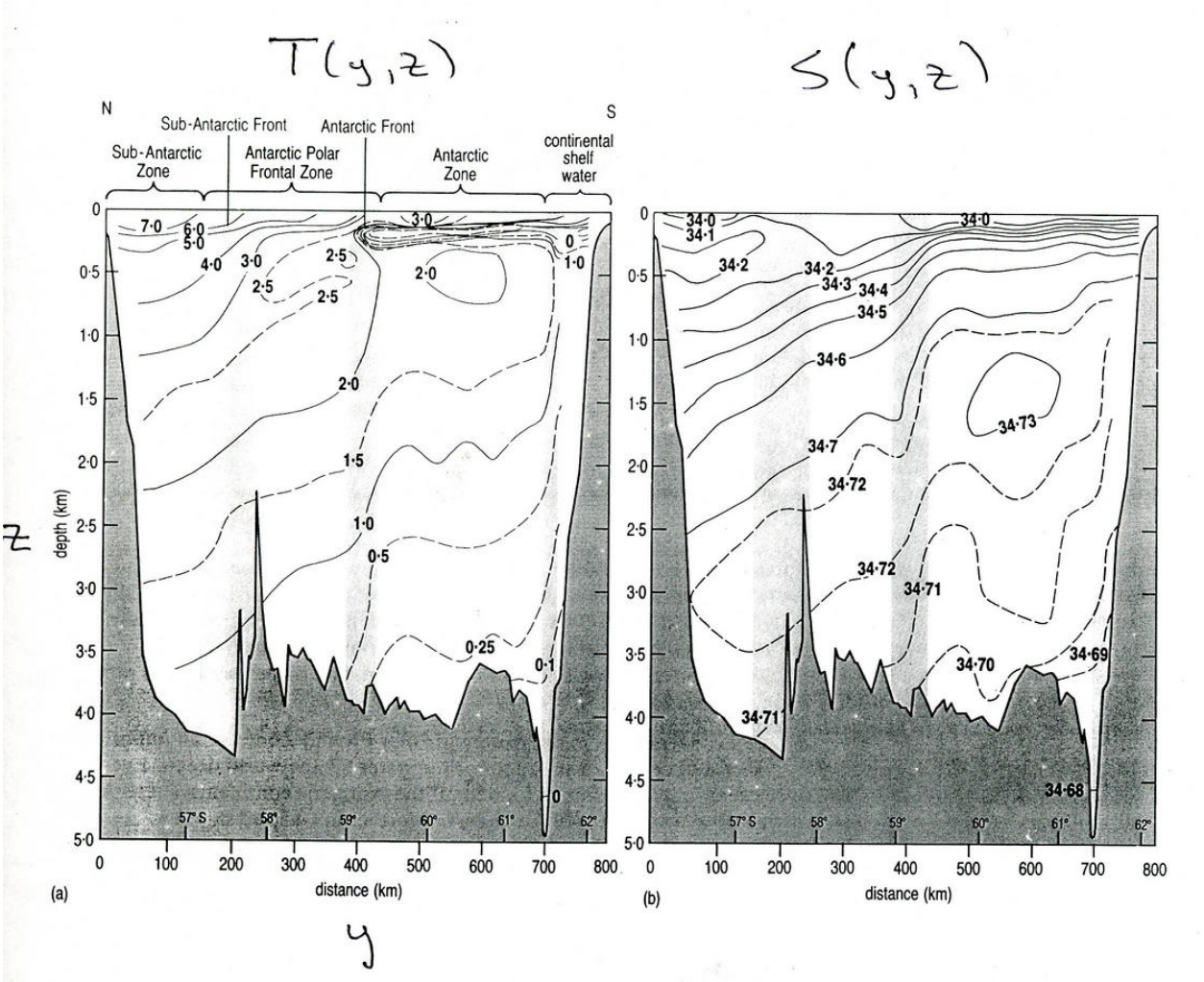

Figure 12: Hydrographic meridional section across the ACC at Drake Passage (Whitworth, 1988).

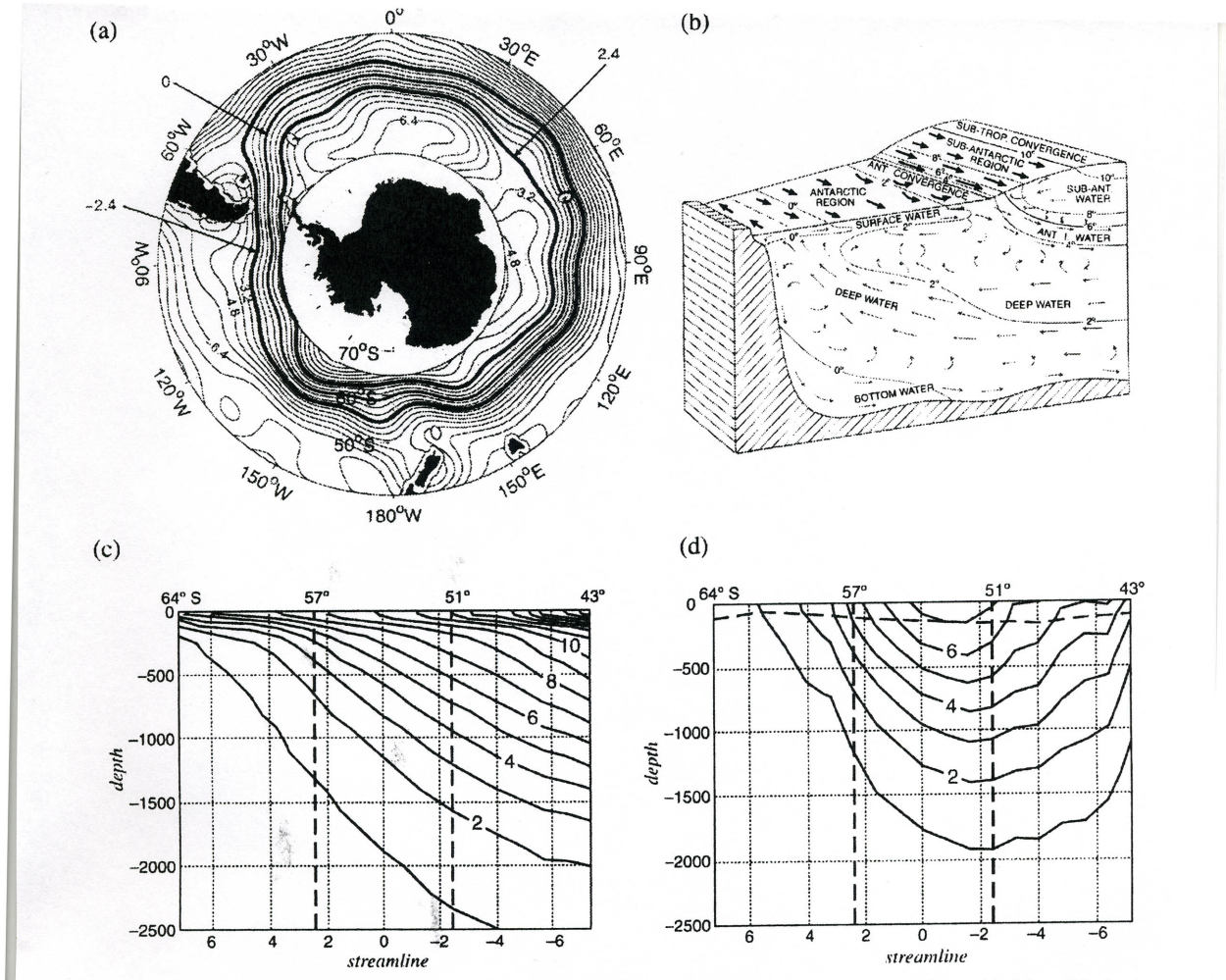

FIG. 1. Key observations of the ACC: (a) the time-mean surface elevation measured from altimetry. Contour interval is 0.8×10^4 m^2 s^{-1}. The bold lines mark the boundaries of circumpolar flow. (b) A schematic of the currents and overturning circulation in the Antarctic region modified from Fig. 164 of Sverdrup et al. (1942). (c) The streamwise-average buoyancy distribution computed from gridded hydrography; contour interval is 10^{-3} m s^{-2}. The vertical dotted lines denote the average latitude of circumpolar flow marked in (a). (d) The thermal wind velocity computed from gridded hydrography by integration of the thermal wind assuming zero current at the bottom; contour interval is 10^{-2} m s^{-1}. Modified from Karsten and Marshall (2002b).

Figure 13: (Marshall and Radko, 2003)

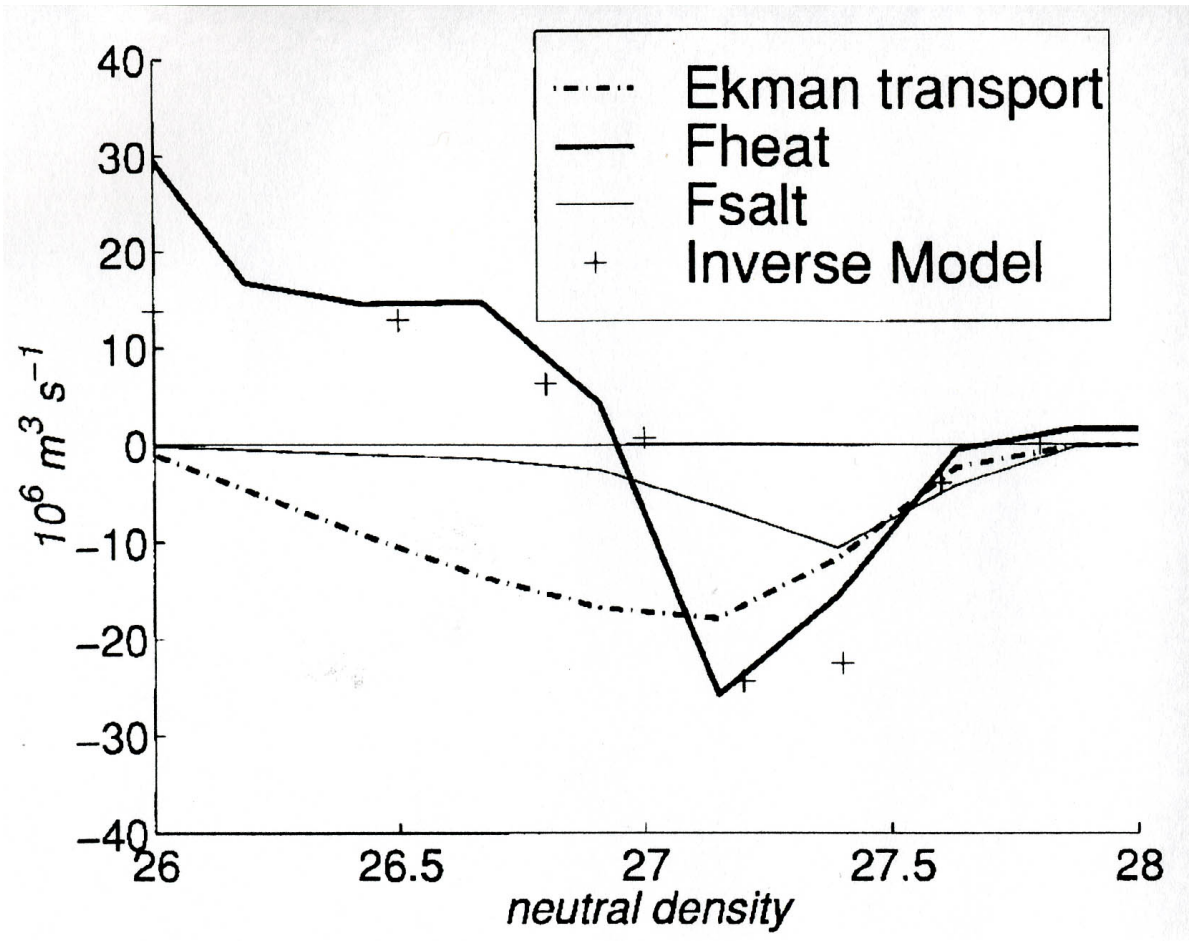

Figure 14: Water mass transformation in the southern hemisphere calculated from COADS (*i.e.,* shipboard) heat and freshwater flux data. A zone of buoyancy gain occurs at surface densities greater than 27 in both components of the buoyancy flux. Ekman transport is shown for comparison, showing the alignment of buoyancy gain and growing northward transport (divergent Ekman flow, hence Ekman suction). Inverse model results for total transformation are generally consistent (Speer et al., 2000).

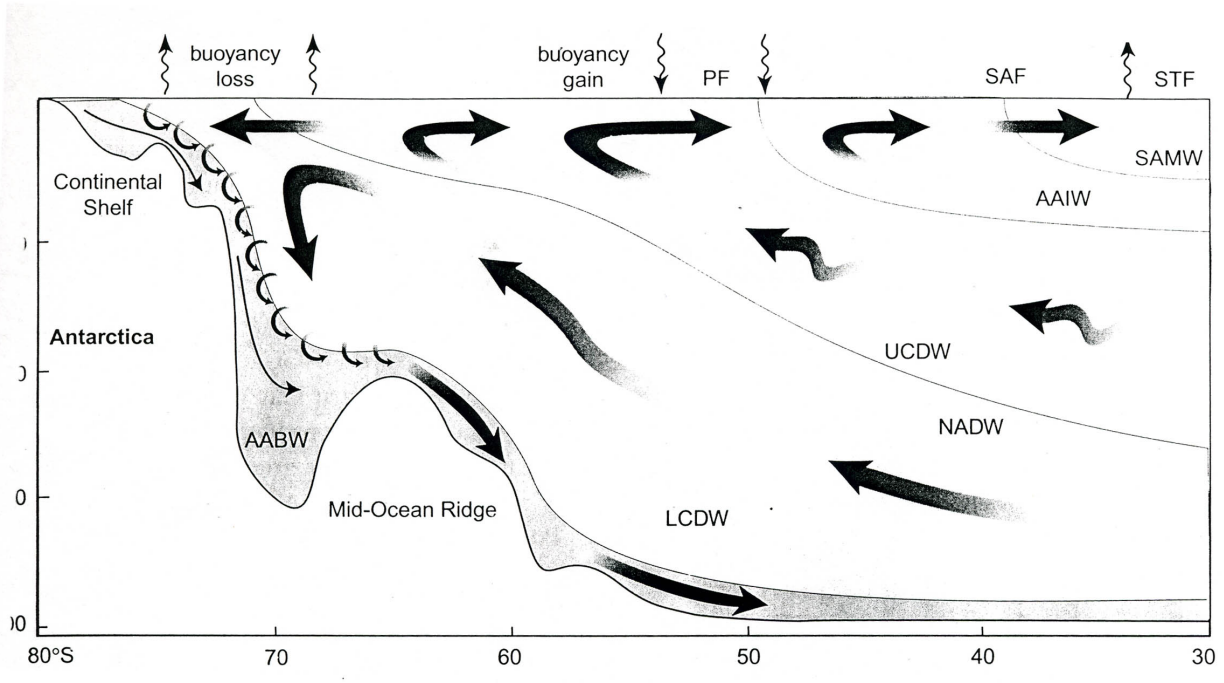

Figure 15: A schematic view of the MOC in the southern ocean. An upper cell is formed primarily by northward Ekman transport beneath the strong westerly winds with an associated upward eddy transport in the UCDW layer. A lower cell is driven primarily by formation of dense AABW near the Antarctic continent. PF=Polar Front; SAF=Subantarctic Front; STF=Subtropical Front; AAIW=Anarctic Intermediate Water; ECDW=Upper Circumpolar Deep Water; NADW=North Atlantic Deep Water; LCDW=Lower Circumpolar Deep Water; AABW=Antarctic Bottom Water. (Speer et al., 2000)

References

Andrews, D., J. Holton, and C. Leovy: 1987, *Middle Atmosphere Dynamics*. Academic Press, 489 pp.

Cai, W. and P. Baines: 1996, Interactions between thermohaline- and wind-driven circulations and their relevance to the dynamics of the Antarctic Circumpolar Current, in a coarse-resolution global ocean general circulation model. *J. Geophys. Res.*, **101**, 14073–14093.

Charney, J.: 1955, The Gulf Stream as an inertial boundary layer. *Proc. Natl. Acad. Sci. USA*, **41**, 731–740.

Danabasoglu, G. and J. McWilliams: 1976, Sensitivity of the global ocean circulation to parameterizations of mesoscale tracer transports. *J. Clim.*, **8**, 2967–2987.

Gent, P. and J. McWilliams: 1990, Isopycnal mixing in ocean circulation models. *J. Phys. Ocean.*, **20**, 150–155.

Lorenz, E.: 1967, *The Nature and Theory of the General Circulation of the Atmosphere*. World Met. Org., 161 pp.

Marshall, J. and T. Radko: 2003, Residual-mean solutions for the Antarctic Circumpolar Current and its associated meridional overturning circulation. *J. Phys. Ocean.*, **33**, 2341–2354.

McWilliams, J. and J. Chow: 1981, Equilibrium geostrophic turbulence: I. a reference solution in a beta-plane channel. *J. Phys. Ocean.*, **11**, 921–949.

Panetta, L.: 1993, Zonal jets in wide baroclinically unstable regions: Persistence and scale selection. *J. Atmos. Sci.*, **50**, 2073–2106.

Speer, K., S. Rintoul, and B. Sloyan: 2000, The diabatic Deacon Cell. *J. Phys. Ocean.*, **30**, 3212–3222.

Toggweiler, R. and B. Samuels: 1998, On the ocean's large-scale circulation near the limit of no vertical mixing. *J. Phys. Ocean.*, **28**, 1832–1852.

Treguier, A. and J. McWilliams: 1990, Topographic influences on wind-driven, stratified flow in a Beta-plane channel: An idealized model for the Antarctic Circumpolar Current. *J. Phys. Ocean.*, **20**, 321–343.

Treguier, A. and L. Panetta: 1994, Multiple zonal jets in a quasigeostrophic model of the Antarctic Circumpolar Current. *J. Phys. Ocean.*, **24**, 2263–2277.

Webb, D. and N. Suginohara: 2001, Vertical mixing in the ocean. *Nature*, **409**, 37.

Whitworth, T.: 1988, The Antarctic Circumpolar Current. *Oceanus*, **31**, 53–58.

Wolff, J.-O., E. Maier-Reimer, and J. Olbers: 1991, Wind-driven flow over topography in a zonal beta-plane channel: A quasigeostrophic model of the Antarctic Circumpolar Current. *J. Phys. Ocean.*, **21**, 236–264.